Int J Earth Sci (Geol Rundsch) (2017) 106:2387–2405
DOI 10.1007/s00531-016-1433-x

ORIGINAL PAPER

Structural pattern and emplacement mechanism of the Neka Valley nappe complex, eastern Alborz, Iran

Seyed Tohid Nabavi[1] · Aziz Rahimi-Chakdel[2] · Mohsen Khademi[3]

Received: 19 November 2016 / Accepted: 3 December 2016 / Published online: 20 December 2016

Abstract The Neka Valley nappe complex is exposed in the south of Gorgan County in the eastern Alborz fold-and-thrust belt. We use the results of a regional survey of the structural data and their patterns to interpret the mechanisms that emplaced the unmetamorphosed nappes in the foreland fold-and-thrust belt of the Alborz Mountains. Most of the strain magnitudes are low in the study area but increase slightly towards what are probably their proximal ends. Strain ellipsoid is dominantly oblate with *XY* aligned along and across the belt (or the nappe complex). The average kinematic vorticity number, $W_k = 0.6$ which indicates most of the strain partitioning resulted in a general shear. Most of Flinn's k values and α (the stretch along the shear plane) values are lower than 1. Structural indicators such as orthogonal extensional joints, pinch-and-swell structures, anastomosing cleavages, and listric normal and growth faults developed by push from the rear. Large-scale thrust complexes with opposed-dips such as triangle zones (as well as k and α-values <1) are compatible with the shear flow diverging distally and streamlines expected of the rear compression emplacement mechanism. Together with a later minor brittle deformation, these major ductile strains appears to provide a general model suitable for the emplacement of the nappes studied in a thin-skinned fold-and-thrust belt where the sedimentary cover strata shortened and imbricated in the upper crust.

Keywords Nappe complex · Emplacement mechanism · Rear compression · Neka Valley · Eastern Alborz

✉ Seyed Tohid Nabavi
Tohidnabavi@gmail.com; T_nabavi@sbu.ac.ir

1 Department of Geology, Faculty of Earth Sciences, Shahid Beheshti University, Tehran, Iran

2 Department of Geology, Faculty of Sciences, Golestan University, Gorgan, Iran

3 Faculty of Earth Sciences, Damghan University, Damghan, Iran

Introduction

Lateral collisional orogenic belts are dominated by lateral contractional structures, such as folds, thrusts and thrust sheets (nappes) that collectively thicken the continental lithosphere (Merle 1998; Mukherjee 2010a, b, 2013a, b, c, 2014a, b, c, 2015; Dubey 2014). Nappes develop by two mechanisms (Henderson and Dahlstom 1959; Talbot 1974; McClay and Price 1981): (1) basal thrust faulting that detaches the first-order (thrust nappe) and (2) regional overturned or recumbent folding categorising it as a second-order fold nappe. Nappes are the brittle–ductile structures fundamental to compressional continental orogens. Many such nappes are in foreland fold-and-thrust Belts (such as Mohand Anticline in NW Himalaya: Biswas et al. 2014) that form above shallow basal detachment surfaces (floor thrust) and undergo high internal deformations above a rigid and undeformed crystalline basement. Lateral tectonic shortening and vertical thickening are recorded by folding and thrusting (and in some cases normal faulting, crustal channel flow and critical tapering: Mukherjee 2005, 2010b, c, 2011a, b, 2014b, d; Mukherjee and Koyi 2010; Mukherjee et al. 2012, 2015; and back deformation: Bose and Mukherjee 2015), that will also affect the length, breadth, depth of Moho and lithospheric thickness (McClay and Price 1981; McClay 1992; Merle 1998; Wissing et al. 2003). The style of deformation in which the basement remains undeformed, is known as 'thin-skinned tectonics'

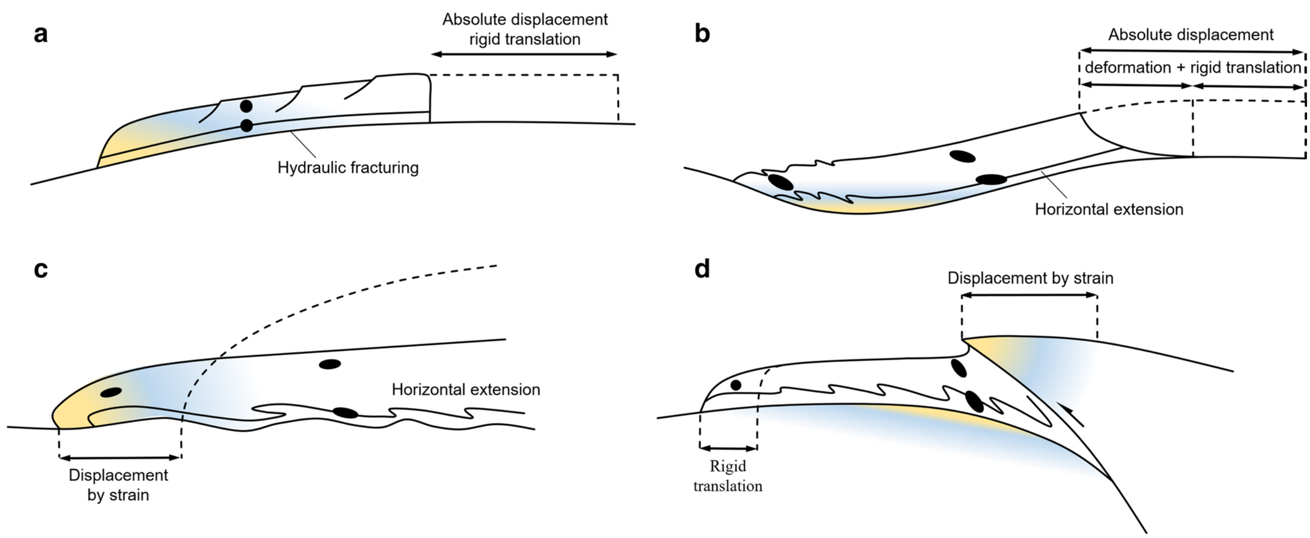

Fig. 1 Mechanical models according to different possible emplacement mechanisms of nappes. **a** Rigid gliding; **b** ductile gliding; **c** gravity spreading or gravitational collapse; **d** rear compression or push from behind. Modified from (Merle 1986, 1998)

in which most of the "cover nappes" verge towards the foreland constituting regional fore-structures/fore-folds (McClay 1992; Escher et al. 1993; Epard and Escher 1996; Plašienka and Prokešova 1996; Pfiffner 2006; Prokešova et al. 2012). Stratigraphic units within nappes may contain markers suitable for useful strain analysis. Coward and Kim (1981) demonstrated that strains in thrust sheets may be subdivided into: (a) layer parallel shear strains, (b) longitudinal strains such as layer parallel shortening (LPS) or extension and (c) layer normal shear strains.

Field, experimental/analogue and mathematical studies have shown that internal strains can be considered to be as a combination of two components of strain (Ramberg 1975a, b; Coward 1976, 1980; Sanderson et al. 1980; Sanderson 1982; Merle and Brun 1984; Sanderson and Marchini 1984; Fossen and Tikoff 1993; Tikoff and Fossen 1993; Ring 1998; Provost et al. 2004; Merle 1998; Ring and Kassem 2007; Mukherjee and Koyi 2010; Mukherjee 2012a, b, 2014b, Frehner 2016; Nabavi et al. 2016b). These components are: (1) a component of pure shear where the stretching α is parallel to the basal plane and relates to either a vertical shortening and a horizontal lengthening ($\alpha > 1$) or to a horizontal shortening and a vertical lengthening ($\alpha < 1$), and (2) a component of heterogeneous simple shear (γ) (also see Vitale and Mazzoli 2015) where the plane of shearing is parallel to the basal plane and the intensity of shearing increases towards the base of the nappe. The directions of ductile shear (or gravity spreading) in plan-form therefore parallel the direction of displacement and can be more or less radial during gravity spreading or largely downslope in the case of gravity gliding. Hence, the most commonly used division of nappes is based on the presence or absence of more competent crystalline basement rocks at or along their bases. Important factors controlling the structural styles of cover nappes are the compositions, the continuities and thicknesses of the weak detachment layers in the nappes and also the lateral extent of stratigraphic units with these characteristics above the basal detachment horizon (Davis and Engelder 1985; Pfiffner 1985, 1993; Jordan 1992; Davis and Lillie 1994; Plašienka and Prokešova 1996; Wissing and Pfiffner 2003; Wissing et al. 2003; Prokešova et al. 2012).

Since the first recognition of nappes in the nineteenth century, their genesis has been of great interest of structural geologists all over the world (see Fig. 1 and Merle 1998 for review). There are four major emplacement mechanisms of nappes: (1) down slope rigid or frictional gliding controlled by Navier-Coloumb criterion of brittle failure (Hubbert and Rubey 1959; Siddans 1984; Plašienka and Prokešova 1996; Talbot and Pohjola 2009; Prokešova et al. 2012; Fossen 2016) (Fig. 1a), (2) ductile or viscous gliding or flow of the whole nappe along of down a low viscosity basal stratum (Hsü 1969; Kehle 1970; Siddans 1984; Brun and Merle 1985, 1988, 1986; Talbot and Pohjola 2009; Fossen 2016) (Fig. 1b), (3) ductile or viscous spreading (extensional flow) of the whole nappe under its own weight (Talbot 1974; Elliott 1976; Ramberg 1977; Siddans 1984; Brun and Merle 1985; Merle 1986, 1989; Ramberg 1989, 1991; Talbot and Pohjola 2009; Prokešova et al. 2012; Fossen 2016) (Fig. 1c), and (4) rear compression (push from behind) (Ramberg 1977; Chapple 1978; Dahlen et al. 1984; Siddans 1984; Cello and Nur 1988; Guillier 1988; Talbot and Pohjola 2009; Prokešova et al. 2012; Fossen 2016) (Fig. 1d). Each of these emplacement imply a different timing of phases of brittle and ductile deformation with respect to the evolving orogen and each should display a different but characteristic morphology and strain distribution within the nappe. Different combination of all these four mechanisms can be classified into several ratios of gravitational and lateral forces and shapes and inclinations of the basal thrust. Identifying the forces that emplaced each/any nappe requires recognition of patterns of foliation trajectories (especially in vertical sections parallel to the displacement direction); finite strain gradients; strain regime (coaxial/non-coaxial or both) (Mukherjee 2012a; Mukherjee and Biswas 2014); displacement gradients; and the relations between stretching lineations and displacement directions (Prokešova et al. 2012). Strains within nappes have been modelled using simple boundary condition (e.g. Ramsay 1981; Pfiffner 1981; Harris et al. 1983; Siddans 1983; Groshong et al. 1984; Siddans et al. 1984; Seno 1992; Fossen 1993a, b; Singh and Jain 1993; Mitra 1994; Burg et al. 1996; Gutiérrez-Alonso 1996; Fowler and El Kalioubi 2004; Pastor-Galán et al. 2009; Thigpen et al. 2010; Sarkarinejad et al. 2015).

Movement of a material volume along a displacement surface over other units creates various components of pure and simple shear that parallel the thrust or glide plane (Mukherjee and Koyi 2010). Hence, the shape and orientation of the finite strain ellipsoid is a critical tool for understanding how particular nappes came into being. Unlike thrust and fold nappes in the rest of the world, little attention has been paid to the nappes in the Alborz Mountain Range, especially the geometries of their patterns of internal deformation/strain. Along with previous research by Nabavi et al. (2016a), this study, therefore, aims to discuss structural field observations and the geometries of measured strains so as to propose a model for the emplacement mechanism of the Neka Valley nappe complex. These issues should certainly be useful to decipher the tectonics of nappes and thrust sheets in the Alborz orogeny.

Geological setting

The Alborz Mountain chain has two "arms" along the northern border of Iran. West of an N–S corridor between 52° and 53°, the East the Alborz Mountains trend W–E, east of that corridor, they trend SW–NE. The Alborz Mountains are ca. 100 km wide and ca. 600 km long along the southern shore of Caspian Sea and accommodate the N–S convergence between Central Iran and Eurasia plates in late Triassic (Jackson and McKenzie 1984) and the NW motion of the South Caspian Basin. These motions have resulted in left-lateral shear to NNE–SSW transpression with thrusting for the last 5 ± 2 Ma (Jackson et al. 2002; Allen et al. 2003; Ritz et al. 2006; Djamour et al. 2010; Javidfakhr et al. 2011; Baikpour and Talbot 2012). Both arms of the orogeny are double-verging as result of the collision of the Iranian plate with Eurasia, starting from the middle to late Triassic Eo-Cimmerian orogeny, which continues as intracontinental deformation related to the present active convergence between the Arabian and Eurasian plates (Alavi 1996; Allen et al. 2003, 2004; Guest et al. 2007; Zanchi et al. 2006, 2009). The Alborz Mountains have been deformed during several tectonic episodes. The first, during the late Triassic, corresponded to the collision of the Iranian plate with Eurasia (Alavi 1996; Berberian and King 1981). The second and more important was the following convergence between Arabia and Iran that continues today. The last event (3 Ma to present) is associated with structural and strain partitioning (Ballato et al. 2008, 2011; Hollinsworth et al. 2008).

The study area is located in the south of Gorgan County, Shah-Kuh area, in the eastern part of the Alborz Mountains Range (Fig. 2a, b) between the Shah-Kuh and Haji-abad thrusts (Fig. 2c). The area includes rock units dating mainly from Devonian to Quaternary rocks exist here. Devonian conglomerates, sandstones, limestones of the Khosh Yeilagh Formation are covered by the Lower Carboniferous Mobarak Formation, with basal limestones passing upward to well-bedded dark limestones at the top. The Middle Carboniferous limestones and oolitic sandy limestone of the Quezel-Qaleh Formation pass upward to carbonate and terrigenous facies. The Quezel-Qaleh Formation occurs at the base of the Permian succession. The Permian successions appear at the base of the red conglomerates, sandstones, silty limestones and limestones with fusulinides that form the Doroud Formation (Zanchi et al. 2009). Bedded to massive limestones of the Ruteh Formation and dolomitic limestones and dolostones of the Elika Formation constitute the upper part of the Permian succession. The Early Jurassic Shemshak Formation includes sandstones, shales, clays and coal, and is followed by continental, lacustrine and lagoonal sequences. The Lower Carboniferous Mobarak Formation is not exposed in the study area but can be found to the northwest, where the sandy and inoceramus-bearing limestones of the Late Cretaceous Ghalemoran Formation unconformably overlies it (Fig. 3a). Folding is a common response to deformation within nappes and thrust sheets. Flexural slip folding formed open semi-cylindrical chevron folds in the Doroud and Elika Formations with upright to steeply inclined axial surfaces, and semi-horizontal to gently plunging axes. Upright and overturned folds on metric to decametric scale wavelengths and amplitudes formed in the Mobarak Formation (Fig. 3b) and Ruteh and Doroud limestones (Nabavi, 2012). Gentle asymmetric folds developed as a result of a break thrust in the Santonian Ghalemoran Formation (Fig. 3c). Most of thrusts that affect the Permian sequences are listric with both stair-step and smooth trajectories; some dip in opposite direction across the orogen (Fig. 3d, e).

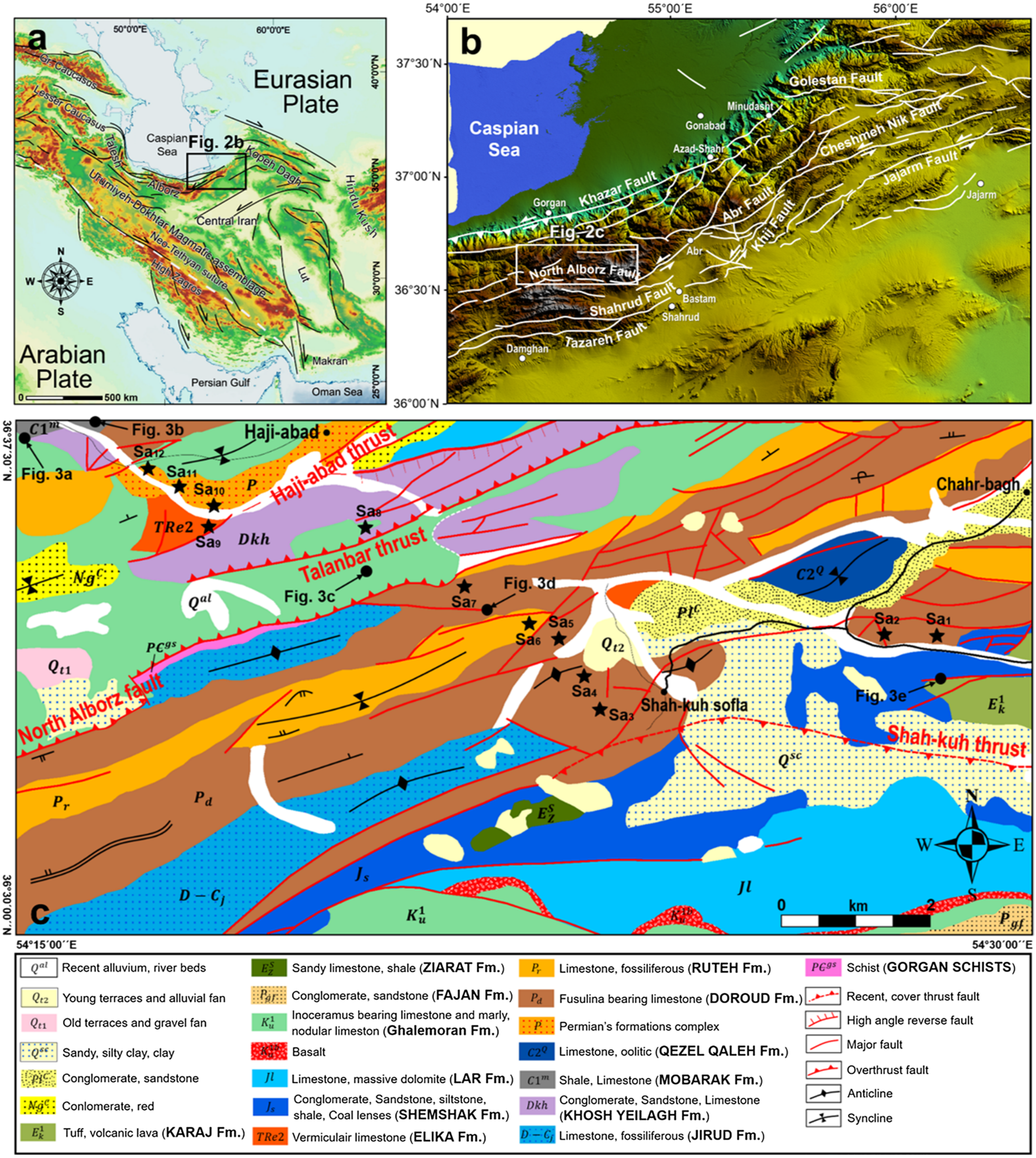

Fig. 2 **a** Simplified map of Iran showing the distribution of major faults. The *rectangle* indicates the study area (**b**), which is located south of Gorgan County; **c** geological map of the study area. Position of the oriented specimens is shown by Sa and filled stars in this map and listed in Table 1. This modified map is part of the 1:250,000 Gorgan quadrangle map from Shahrabi (1990)

Materials and methods

Twelve oriented hand specimens were collected from different locations and Formations (identified in Fig. 3c by star symbols and listed in Table 1) to measure the finite strains using the Fry technique (Fry 1979). Our two-dimensional strain data measurements used the Fry Plot Program (Roday et al. 2010; http://fry-plot-program.software.informer.com/). We also used

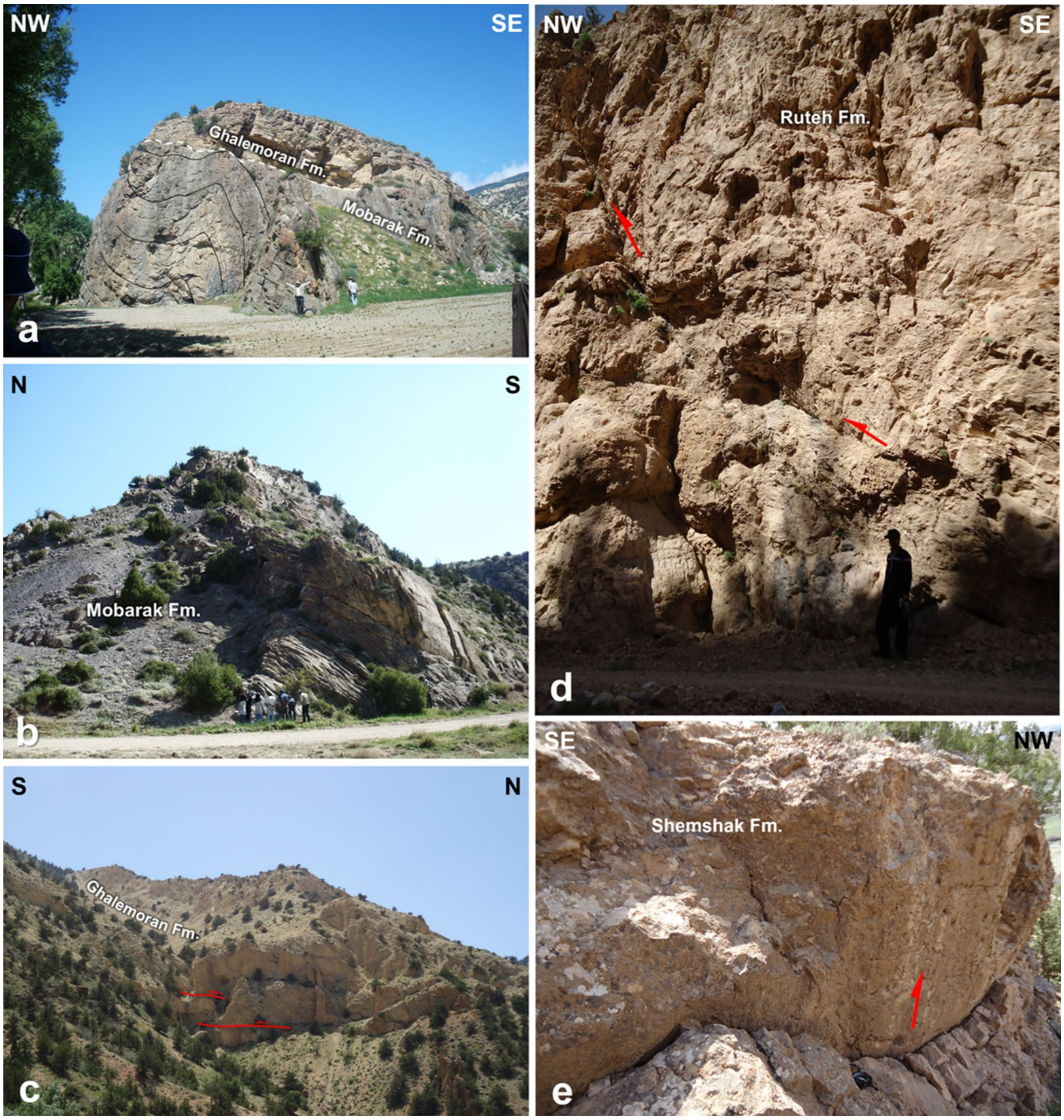

Fig. 3 **a** A view of late Cretaceous unconformity where the Ghalemoran Formation overlies the folded Mobarak Formation; **b** overturned folds on metric to decametres scale wavelengths and amplitudes formed in the Mobarak Formation; **c** a break thrust in the Ghalemoran Formation, Haji-abad area; **d** *upper part* of a listric thrust fault in the Ruteh Formation that follows a staircase or stair-step trajectory; **e** a listric thrust fault in the Shemshak Formation, Shah-Kuh area

Rod J. Holcombe's Strain and Shear Calculator 3.2 Program (http://www.holcombe.net.au/software/straincalculator.html) to calculate and plot strain data using a variety of input parameters, to simulate simple shear, pure shear, and general shear, while showing all the related parameters. Our data measured in appropriate 2D profiles were integrated to 3D strain data. Three-dimensional strain intensities (ε_s and D), Lode's parameter (ν) and logarithmic Flinn's parameter (K) are calculated by:

$$\varepsilon_s = \frac{1}{\sqrt{3}}\left[(\ln X/Y)^2 + (\ln Y/Z)^2 + (\ln X/Z)^2\right]^{1/2} \quad (1)$$

$$D = \sqrt{\ln(R_{XY})^2 + \ln(R_{YZ})^2} \quad (2)$$

$$\nu = \left(\log Y/Z - \log X/Y\right)/\left(\log Y/Z + \log X/Y\right) \quad (3)$$

$$K = \frac{\ln(R_{XY} - 1)}{\ln(R_{YZ} - 1)} \quad (4)$$

The results were plotted on logarithmic Flinn and Nadai/Hsü graphs (Flinn 1962; Nadai 1963; Hsu 1966; Ramsay and Huber 1983).

Table 1 Strain parameters calculated from deformed samples

Sample	Lithology	Formation	Dist. (m)	R_{XZ}	R_{XY}	R_{YZ}	k	θ'	γ	α
1	Limestone	Doroud	11,000	2.95	1.45	2.03	0.43	33	1.21	0.88
2	Fusulina-bearing limestone	Doroud	10,700	3.07	1.446	2.12	0.4	33	1.29	0.9
3	Fusulina-bearing limestone	Doroud	6640	2.75	1.434	1.91	0.48	36	1.09	0.9
4	Limestone	Doroud	6200	2.6	1.45	1.7	0.64	36	1.02	0.87
5	Ooid-bearing limestone	Doroud	3250	2.5	1.453	1.71	0.64	37	0.95	0.87
6	Sandy limestone	Ruteh	2670	2.43	1.45	1.67	0.67	37	0.88	0.89
7	Ooid- and fusulina-bearing limestone	Doroud	1080	2.15	1.431	1.6	0.71	34	0.78	0.98
8	Inoceramus-bearing limestone	Ghalemoran	55	2.1	1.44	1.45	0.98	36	0.62	0.94
9	Vermicular limestone, dolomite	Elika	2445	2.05	1.444	1.41	1.08	37	0.68	0.93
10	Limestone	Permian complex	2300	2.69	1.451	1.85	0.53	35	1.05	0.88
11	Limestone	Permian complex	2630	2.51	1.45	1.73	0.64	37	0.95	0.87
12	Limestone	Permian complex	3100	2.77	1.447	1.9	0.5	33	1.09	0.94

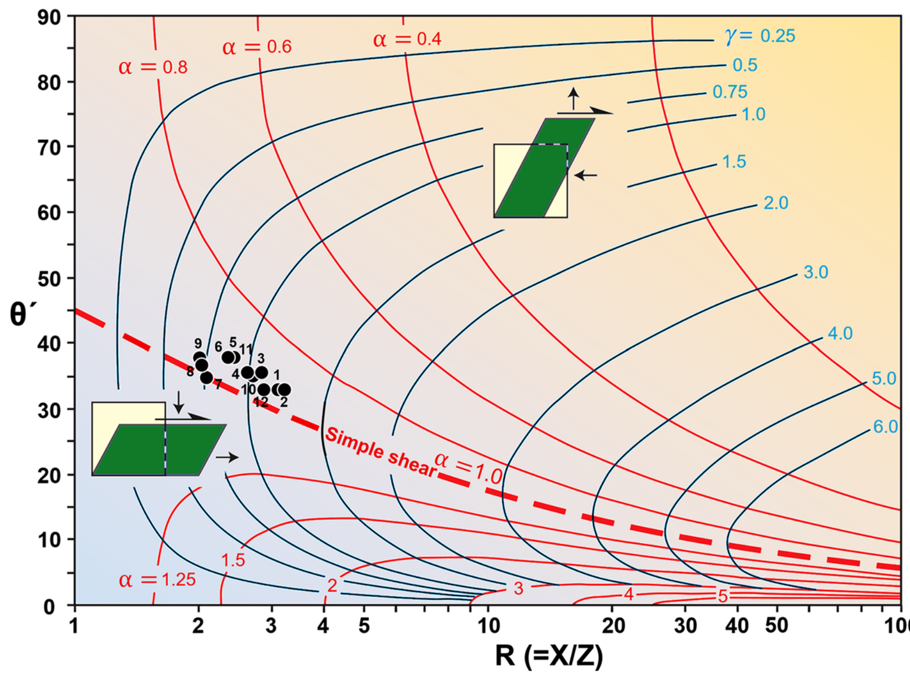

Fig. 4 R–θ' diagram for zones affected by simultaneous simple and pure shear. R is the strain axes ratio and θ' is the angle between the shear plane or zone and the long axis of the finite strain ellipse. The *blue lines* are contours of constant simple shear (γ) values, while the *red lines* show constant pure shear (α). The simple shear curve starts at $\theta' = 45°$. Note that and only the horizontal axis is logarithmic (after Tikoff and Fossen 1993). The *black* points plot our strain data; most ellipsoids plot above the simple shear curve ($\alpha = 1$) and in the ranges of $\alpha = 0.8$–1 and $\gamma = 0.7$–1.2

Discussion

R–*θ′* diagrams and emplacement mechanism

In order to discuss a realistic model for the emplacement of the nappes we studied, we used techniques described by Coward and Kim (1981), Kligfield et al. (1981), Sanderson (1982), Fossen and Tikoff (1993), Tikoff and Fossen (1993) and Merle (1998) to consider all possible combination of simple and pure shear (i.e. general non-coaxial shear). We treated our measurements of deformed ooids and fossils as giving both the shapes and orientations of the finite strain ellipses and ellipsoids in our samples. We plot our data on a graph of the orientation, θ', of the maximum finite elongation, X, against the strain magnitude, R (Fig. 4). On this diagram, contours of pure shear component (α) and shear strain (γ) plot as two intersecting sets of curves. The strain of several points across a shear zone plotted on the R–θ' diagram will often define a line. It has been argued that this line is a very good proxy for the strain path followed by the sample rocks in the study area (e.g. Bhattacharyya and Hudleston 2001). Stretch in the y-axis (α_y) depends on α and α^{-1} such that the R–θ' diagram state of strain provides no insight into the magnitude of α_y (Bhattacharyya and Hudleston 2001; Baird and Hudleston 2007; Samani 2015). Figure 4 can be used to constrain the proportions between the two components of α and γ which will help comment on the mechanisms of emplacement the

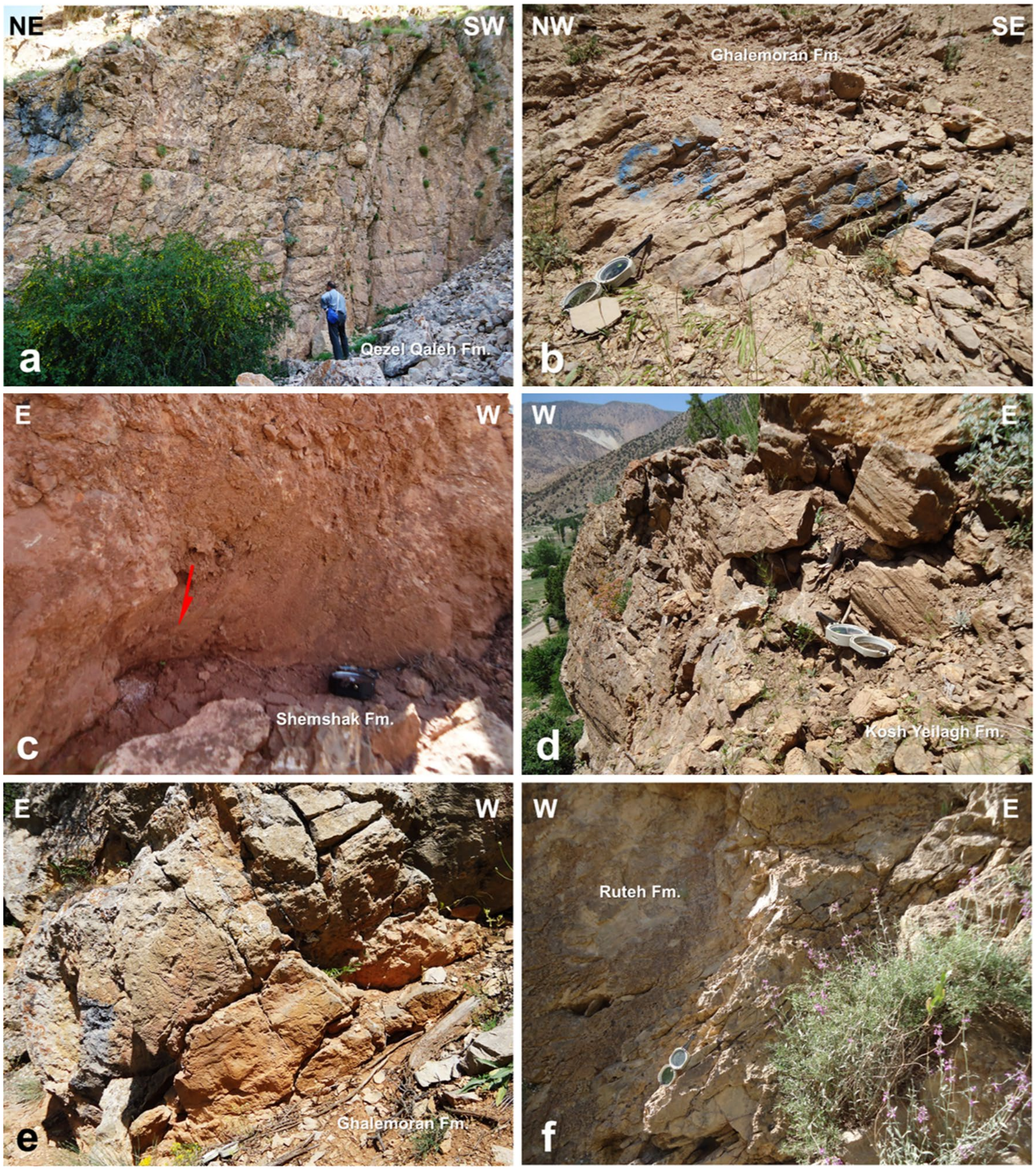

Fig. 5 Some of individual structures related to the rear compression emplacement mechanism in the Neka Valley nappe complex. **a** Orthogonal extension joints in the Qezel Qaleh Formation, Chaharbagh area; **b** pinch-and-swell structure in Ghalemoran Formation. **c** Listric normal faulting in the Shemshak Formation, Shah-Kuh area; **d** left-lateral strike-slip faulting in the Khosh Yeilagh and Ghalemoran Formations; **e** orthogonal extensional fracture on the strike-slip fault plane in the Ghalemoran Formation, Haji-abad area; **f** anastomosing cleavages and symmetric boudin in the Ruteh Formation

nappes we consider (e.g. Coward 1980; Sanderson 1982; Merle 1986; Fossen and Tikoff 1993; Tikoff and Fossen 1993).

For the all samples of the study area, the *XZ* axial ratios and the angles between the *X* axes and the shear plane were plotted on the strain chart in Fig. 4. Figure 4 plots the θ' against *R* for all the strain ellipsoids measured from the study area; they all lie in $\alpha < 1$ field. The shear strains are all low ($0.62 \leq \gamma \leq 1.29$), homogeneous and oblate. The following individual structures photographed in Fig. 5 are relevant to constraining the emplacement mechanism of nappes: (1) orthogonal dilation (extension) joints in the Qezel-Qaleh Formation are attributed to bidirectional horizontal NE–SW extension (Fig. 5a). Planar dilation joints that intersect along the inflection point of folds and dilation joints fanning from the hinges of angular folds indicate brittle buckles of competent beds (Frehner 2011; Frehner and Exner 2014). This is in addition to the development of dilation joints in other beds and folds in areas nearby. (2) The long axes of the necks in pinch-and-swell structure in the Ghalemoran Formation trend NW–SE perpendicular to the northeast–southwest extension direction (Nabavi 2012) (Fig. 5b). In addition, there is listric normal faulting in the Shemshak Formation (Fig. 5c), left-lateral strike-slip faulting in the Khosh Yeilagh and Ghalemoran Formations (Fig. 5d), orthogonal extensional fracture on the strike-slip fault plane in Ghalemoran Formation (Fig. 5e), and shear elements and anastomosing cleavages and symmetric structures in shear zones in the Ruteh Formation (Fig. 5f). In addition, upright folds that result from LPS are as a proof of rear compression mechanism (see Fig. 4c in Nabavi et al. 2016a). All the individual group of structures on Fig. 5 are the products of combined divergent (or extensional) flow and shear strains (see Fig. 6a). The mechanism of emplacement being by rear compression is anticipated to result in patterns of strain like the combination of divergent (as streamlines diverge from one another or orthogonal extension, coaxial deformation, flattening strain, and no volume change), and shear flow (streamlines are parallel, and non-coaxial deformation) streamlines seen in Fig. 6a. Our field measurement indicates $\alpha < 1$ and $k < 1$ (Fig. 4; Table 1), suggesting that these emplacement mechanism of the Neka Valley nappe complex was rear compression (push from behind). Therefore, on Fig. 4, the concave curves in the model of rear compression are interpreted on the constant α curve by the increase in the component γ from top towards the base. In two dimension, this emplacement mechanism relates to the case where the pure shear component α is <1 and Flinn parameter k is also <1 (Sanderson 1982; Merle 1986). Therefore, the allochthonous unit thickens towards the source of compression in the rear.

The numerical simulations introduce a gradient in the component α which decreases progressively from the rear towards the front (Fig. 6b) (Guillier 1988). The component of simple shear increases towards the base in many nappes, probably reflecting deformation of more viscous hangingwall rocks just above the thrust (Mitra 1994; Yonkee 2005; Yonkee et al. 2013), although similar increases in basal shears occur in glaciers, ice caps, salt glaciers and experiments with uniform materials (Hudleston 1976, 1977, 2015; Talbot 1979; Hudleston and Hooke 1980; Brun and Merle 1988; Merle 1998). Thus, this mechanism must occur by a combination of shear and divergent flow. The shear strain is zero at the top of nappe where horizontal shortening causes the maximum stretch axis to be vertical (Sanderson 1982; Merle 1986). Horizontal stress applied by the rear compression mechanism ensures that folds are particularly well developed within the rear of the allochthonous unit (Fig. 6c). Upright folds that form in the upper parts (the Doroud and Ruteh Formations) are transformed to the overturned and recumbent folds along the Mobarak and Khosh Yeilagh Formations (Fig. 3b) in the basal zone. Hence, the axial planes of folds define a concave upward shape from the summit towards the base (e.g. Gray and Willman 1991). These changes in folding are related to an increasing strain and simple shear towards the rear or older units of the nappes complex (Fig. 9b in Nabavi et al. 2016a). Following Ramsay and Wood (1973), defining the lengths of the principal strain axes, a logarithmic strain plot is contoured for possible volume change in Fig. 7. According to this diagram, the Neka Valley nappe complex might have experienced a volume loss (dilation) of 0–30%. Although not representing absolute values, Fig. 7 indicates that relative volume loss increased with depth and towards the rear. Such volume losses would be consistent with a transpression dominant geometry ($K \neq 1$) (e.g. Dias et al. 2003; Nabavi et al. 2016a, b). The rear compression mechanism requires the formation of a crustal-scale shear couple that may detach completely the hangingwall from the footwall units, particularly at crustal levels where deformation is likely to be brittle. In addition, NW–SE shortening was restricted to the hangingwall and produced km-scale southeast verging nappes with frontal zones of crumpled upright folds. This condition is consistent with a rear compression mechanism of nappe emplacement with the simple shear component of deformation increasingly accommodated within the hangingwall, down dip towards the core of the orogen.

Strain ellipsoid shape and strain intensity

One of the usual goals of kinematic analysis is to find the dimensions and orientation of the axes of the finite strain ellipse (Sarkarinejad et al. 2010). 2D and 3D Flinn diagrams (1956, 1962, 1979) were used to determine the strain ellipses and ellipsoid types in the Neka Valley nappe complex. According to Hossack (1968), this classification is called strain symmetry. Flinn's k value defines the ratios of the principal strains and distinguishes the different shapes of the strain ellipsoid, i.e. constriction or flattening. Apparent flattening and plane strain predominate in the outer weakly deformed zones, while apparent constriction, especially with higher principal stretching strain, occurs mainly in the central zone of intensive deformation. This suggests that strain patterns are closely related to deformation intensity. See Talbot (2014) for a wide review of the homogeneous and heterogeneous strains and related strain ellipsoids in some gneiss regions.

Two of our ellipsoids plot on the $k = 1$ plane representing shears strains, while the remainder plot in the field of

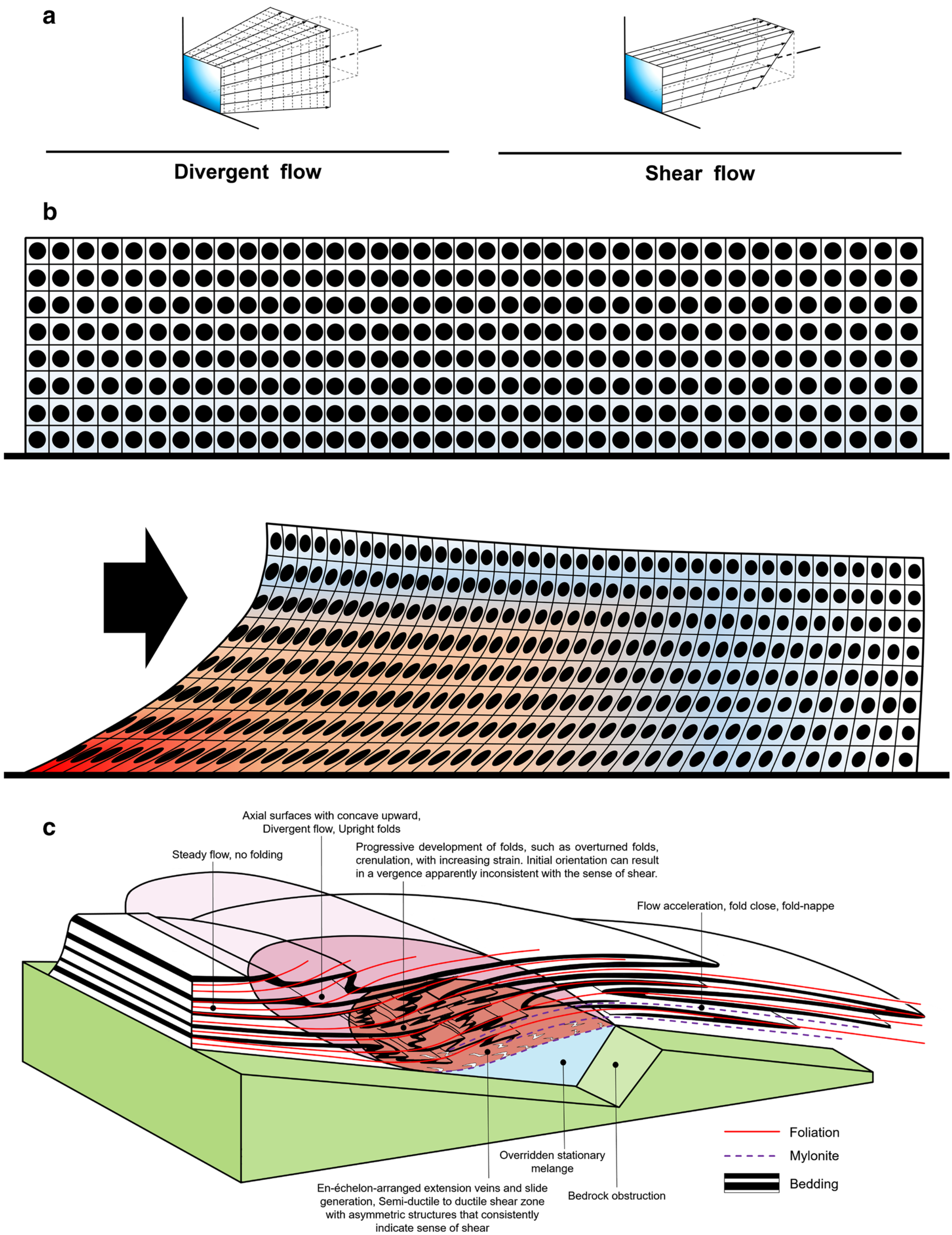

Fig. 6 **a** Streamlines patterns and flow geometries in the rear compression mechanism. Rear compression emplacement mechanism is a combination of divergent and shear flows. In divergent flow, the streamlines all diverge in the downstream direction and so the velocity decreases downstream. In shear flow, the streamlines are all parallel, and the velocity is constant. The velocity of the upper surface, however, is the highest, and of the lower surface the lowest (after Twiss and Moores 2007). **b** Deformation of grid-with-circles obtained numerically from the distribution of the two components α and γ in the two-dimensional models of rear compression (modified from Guillier 1988). **c** Schematic block diagram indicated the Neka Valley nappe complex emplacement with rear compression in early stages of deformation and gravity spreading during next stage (modified after Talbot and Pohjola 2009)

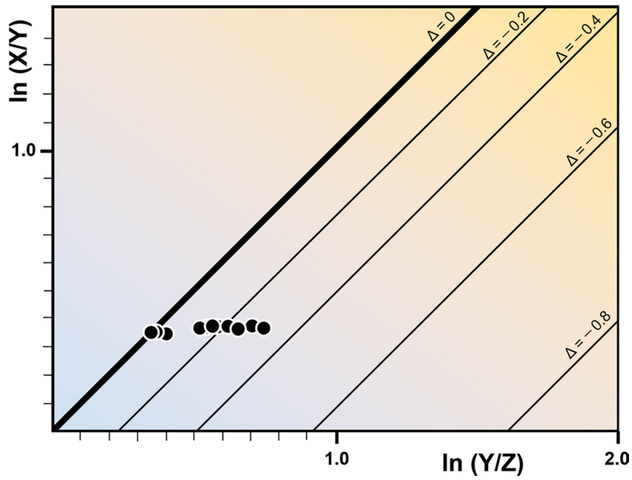

Fig. 7 Contours of volume change (Δ) in a logarithmic strain-shape plot (after Ramsay and Wood 1973)

apparent flattening field ($K = 0.5$–1.06) with D values that range 0.5–0.83 (Fig. 8a). Table 1 lists the lengths of the principal axes of strain. The three-dimensional strain parameters (Table 1), i.e. strain intensity and shape of the strain ellipsoid, can be defined by using the parameter ε_s (Eq. 1) k and ν. Strain magnitude is quantified by ε_s from Nadai (1963) (Fig. 8b). This parameter is useful because it allows comparison of strain magnitude from deformations with different strain paths (Nadai 1963; Hsu 1966; Hossack 1968; Owens 1984; Brandon 1995). A plot of strain data on the k (vertical axis) versus ε_s (horizontal axis) graph reveal the general tendency of our measured strain ellipsoid to flatten more as the strain intensity increases ($\varepsilon_s = 0.504$–0.808) (Fig. 8c). The stretch in the Z direction indicates 31–47% vertical shortening. Data plot on the modified Hsu (1966) graph (Fig. 13 in Talbot and Sokoutis 1995; Talbot 2014) shows 60°–90° plunge for X axis. A plot of k values versus stretches of principal axes of strain (Table 2) shows that one of our strain ellipsoids is prolate, with all the others being oblate (Fig. 8d).

Ring and Kassem (2007) and Abdelsalam (2010) argued that flattening can be associated with nappe emplacement. The $k = 1$ value indicates plane strain, which can be either pure or simple shear. It has been argued that strain symmetry or magnitude depends mostly on metamorphic temperature (Toriumi 1985; Toriumi and Noda 1986) so that oblate strain ellipsoids characterise unmetamorphosed (like the Neka Valley) and lower grade metamorphic (such as Gorgan Schists in green schist facies, to the north of the study area) (Rahimi-Chakdel and Raghimi 2014) rocks in collision-type orogenies such as Alborz Mountains range, while prolate strain ellipsoids are found in higher-grade metamorphic rocks and Cordilleran-type orogeny. Flattening strain can be produced by volume loss, as previously noted, and constriction by volume gain or rotation (Talbot and Sokoutis 1995; Moriyama and Wallis 2002; Talbot 2014). Due to volume changes, changes in the shape and orientation of the material lines relative to a reference line after the deformation, changes in the strain magnitude, also due to kinematic vorticity number (W_k), amount of strain intensity varies in the footwall and hangingwall (nappes) blocks, and state of strain (strain ellipse or ellipsoid) varies within the area. Variation in k values with respect to ε_s reflects the heterogeneous nature of deformation, which in the study area ranges from approximately simple shear to non-coaxial flattening strain (e.g. O'Hara 1990, Capponi et al. 2003; Ring and Kassem 2007; Vitale and Mazzoli 2008, 2010, 2015; Tripathy et al. 2009; Kassem and Abd El Rahim 2010). The origin of strain heterogeneity can be related to temporal evolution of an active deformation zone as (Vitale and Mazzoli 2008, 2010).

The flattening field is characterised by cylindrical folds, probably with boudinage and cross-jointing parallel and perpendicular to the fold hinges, respectively (Ramsay 1967; Frehner 2011); we found such structures in the Ghalemoran, Ruteh and Doroud Formations. The Gorgan schists are mainly slates and phyllites in nappes nearer the hinterland (to the north of the study area) were typically deformed at higher temperatures (Zanchi et al. 2009; Rahimi-Chakdel and Raghimi 2014). Higher temperatures complicated the internal deformation patterns that include components of simple shear, and pure shear (Coward and Kim 1981; Sanderson 1982; Mitra 1994; Seno et al. 1998; Yonkee 2005; Yonkee et al. 2013). Figure 8d indicates that all but one of our strain ellipsoid from the Neka Valley nappes are oblate. Three things stand out from Fig. 8: (1) the ε_s values normally remain quite low (<0.8) throughout the nappe, (2) the intensity of the strain increases with increasing Lode's parameter or decreasing k (Fig. 8c), and (3) the dominance of oblate strain ellipsoids suggests a pure shear model for the study nappe complex. It is also obvious that there is a gradual increases in heterogeneous strain towards the rear (i.e. NNW) and that the shear zone widens away from the nappe boundaries (e.g. Aoya and Wallis 2003; Vitale and Mazzoli 2009, 2015).

Similar patterns have been observed in many thrust sheets in fold-and-thrust belt throughout the world (Fig. 9). Our strain analyses (Fig. 9b in Nabavi et al. 2016a) indicate that the sectional α and W_k increase, whereas γ decreases towards the front with increasing distance from the rear. The variation of α is small compared to that of γ. The strain increments from the back to the front of the nappes reflect an increase in the non-coaxial component of the deformation. This gradient may be included by the gravity-driven movements of the flow. We follow Abad et al. (2003) and

Fig. 8 **a** Logarithmic Flinn plot showing amount and symmetry of ▸ strain found by Fry analysis as *black dots*. The plotted data show k value =1 for shear and <1 for triaxial oblate ellipsoids. **b** Nadai/Hsu (1963) or Hossack's (1968) radial diagram plots show strain ellipsoid distortion (strain magnitude) (ε_s) versus shape or symmetry as Lode's factor (ν). **c** Plot co-coordinate graph plot of k versus ε_s with data. **d** Plot of strain symmetry versus stretches of principal strain axes shows negative correlations for X and Y and a positive correlation for Z

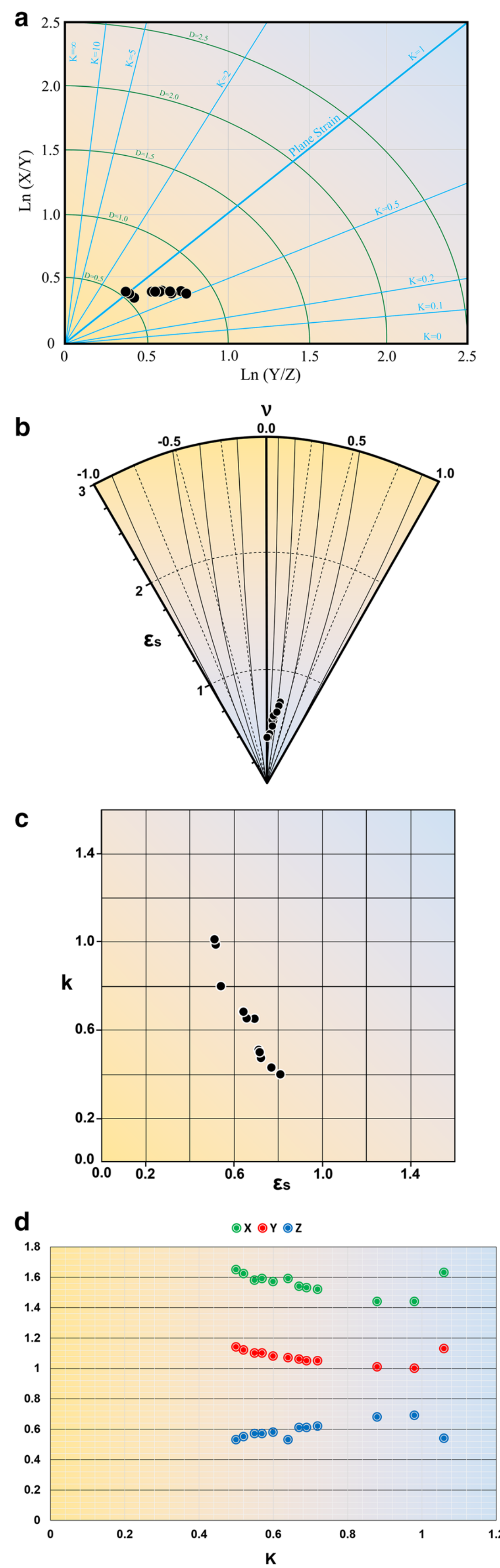

attribute the increase in strain close to the major thrust faults to the simple shear component increasing towards the faults. This variation in strain in the nappe profile may be related to the combination of different movements between the frontal and lateral tips to a major thrust zone, as shown by Lagarde and Michard (1986). This pattern can also be attributed to spatial proximity to several active thrust faults or minor shear zones, as well as superposed emplacement mechanisms. Fissler (2006) and Pastor-Galán et al. (2009) have shown that regional-scale variations in strain magnitude cannot be linked to changes in the concentrations of clast types and petrographic parameters such as grain size, sorting, percentage of matrix, carbonate or feldspar content within their outcrops. Therefore, their low strain values could be due to thin-skinned tectonics, brittle deformation, the existence of splay reverse faults between the two major thrusts, and/or thermal relaxation that led to a low-temperature dynamic metamorphism and more brittle deformation after the Neka Valley nappe complex was emplaced at higher temperatures. Therefore, our low strain values indicate that the study nappes can only have undergone stretching and thinning (Bhattacharyya and Mitra 2009).

The determination of W_k allows us to interpret the emplacement of the Neka Valley nappes in terms of flow mechanics: pure shear (planar extensional) flow, simple shear flow and hyperbolic flow. The flow type may also be determined whether the angle θ' between the flow asymptotes and streamlines is known. In the Neka Valley, nappes θ' ranges 32°–43° and decreases from the front to the back. All of our data (Fig. 8) fall in the field of the hyperbolic flows ($0° < \theta' < 90°$) and depict a roughly continuous trend fitting an empirical power law. This conclusion leads to important implications. The data confirm that the Neka Valley nappes advanced by a rear compression transport model. Internal deformation developed during rear compression and every other emplacement mechanisms ($\alpha < 1$). In addition, some particular structures provide a key to this mechanism. These are the orthogonal extensional joints, pinch-and-swell structures, listric normal growth faults which develop by push from the rear, shear senses and left-lateral shear displacement along Talanbar thrust, symmetric structures in shear zone with nearly straight tails that develop in and compressive shear (e.g.

Table 2 Stretches in the X, Y and Z directions

Sample	X	Y	Z	lnX/Z	lnY/Z	lnX/Y	K	D	ν	ε_s
1	1.623	1.12	0.55	1.081	0.71	0.37	0.52	0.8	0.31	0.775
2	1.65	1.14	0.53	1.121	0.752	0.368	0.5	0.83	0.33	0.808
3	1.58	1.1	0.57	1.011	0.65	0.36	0.55	0.74	0.29	0.724
4	1.59	1.07	0.53	0.953	0.582	0.371	0.64	0.65	0.21	0.679
5	1.53	1.05	0.61	0.913	0.538	0.373	0.69	0.65	0.18	0.648
6	1.52	1.05	0.62	0.884	0.513	0.37	0.72	0.63	0.16	0.627
7	1.44	1.01	0.68	0.764	0.405	0.358	0.88	0.59	0.06	0.54
8	1.44	1.00	0.69	0.735	0.37	0.364	0.98	0.52	0.01	0.519
9	1.63	1.13	0.54	0.713	0.346	0.367	1.06	0.5	–0.03	0.504
10	1.57	1.08	0.58	0.988	0.616	0.372	0.6	0.72	0.25	0.705
11	1.54	1.06	0.61	0.919	0.548	0.37	0.67	0.66	0.2	0.653
12	1.59	1.1	0.57	1.011	0.641	0.369	0.57	0.74	0.25	0.723

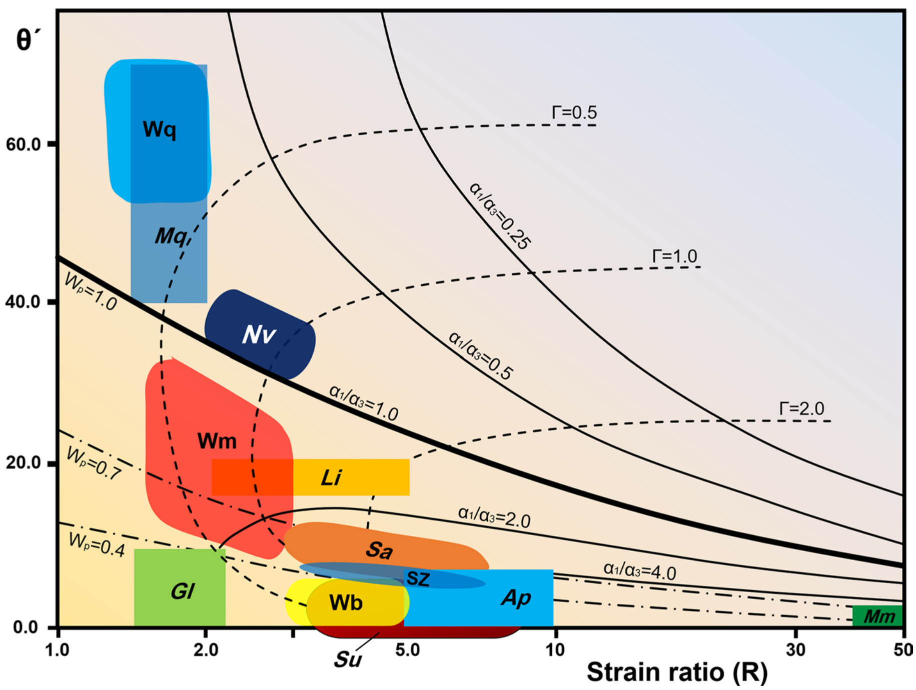

Fig. 9 Plot of R_S (X/Z) versus θ' data from this study (is in *dark blue* patch labelled "Nv") compared to data compiled from studies of thrust sheets in different orogens (Wq, Mq, Wm, Li, Ap, Mm and Wb), transpressive belts (Su and Sa) and shear zones (SZ); modified from Yonkee (2005). Contours of thrust-parallel shear plane (Γ), ratio of thrust-parallel to thrust-perpendicular stretch (α_1/α_3), and mean kinematic vorticity for plane strain (W_p) shown. Typical values for the Neka Valley nappe complex (Nv, *dark blue*) lie in dark blue patch labelled Nv. Abbreviation and data sources: Wq (*light blue*)—micaceous to arkosic quartzite at intermediate levels of Willard thrust sheets, Sevier fold-thrust belt (Yonkee 2005); Wb (*yellow*)—basal levels of Willard thrust sheet (Yonkee 2005); Mq (*blue*)—Moine thrust quartzite (Coward and Kim 1981); Mm (*dark green*)—Moine thrust mylonite zones (Sanderson 1982); Gl (*light green*)—Glarus thrust greywacke (Ring et al. 2001); Ap (*light blue*)—Northern Appenine limestone (Kligfield et al. 1981); Li (*orange*)—Ligurian Alps meta-conglomerate (Seno et al. 1998); Su (*dark red*)—Superior Province belt (Czeck and Hudleston 2003); Sa (*brown*)—Sambagawa belt (Wallis 1995); SZ (*blue*)—examples from various shear zones (Eyster and Bailey 2001). All results indicate the importance of sub-simple shear

Zwart 1974; Gee 1978; Mukherjee 2016a), and opposed-dip large-scale thrust complexes such as the triangle zone, defined by the Shah-Kuh thrust and its related minor thrusts in relying on the Talanbar, Haji-abad and Radekan thrusts.

Comparison of the Neka Valley nappe complex with thrust sheets in other orogens

According to the ratio of pure and simple shear components, the Neka Valley nappe complex deformed mainly by pure shear (Fig. 9). Local strain patterns in the study area record sub-simple/general shear as found in studies of many other thrust sheets (Coward and Kim 1981; Kligfield et al. 1981; Sanderson 1982; Seno et al. 1998; Ring et al. 2001; Yonkee 2005, Long et al. 2011; Yonkee et al. 2013), transpressive belts (Wallis 1995 Czeck and Hudleston 2003) and shear zones (Talbot and Sokoutis 1995; Eyster and Bailey 2001; Carosi et al. 2016). Such similar strain patterns probably reflect shared mechanical processes. The differences in strain patterns between different thrust sheets probably signal such different environmental factors as: temperatures, fluid pressures, lithologies, and boundary conditions. Thrust sheets vary from having broad zones of distributed strain in thick intervals of weak rock (Gray 1995), to having narrow zones of strain concentrated near faults where thick intervals of strong rock are present (Mitra and Boyer 1999). Unmetamorphosed, external thrust sheets (like the Neka Valley nappe complex) typically have only limited LPS and minor simple shear concentrated along their bases and along independent weak units or horizons. LPS can be a significant internal strain mechanism in unmetamorphosed thrust sheets (Coward and Kim 1981; Wojtal 1986; Mitra 1994; Yonkee 2005). According to Hatcher and Hooper (1992) and Hatcher (2004), there are three principal types of thrust in orogenic belts: (1) foreland fold-and-thrust belt thrust sheets or thrust models (e.g. Platt 1986; Schmalholz et al. 2014), (2) type C crystalline thrust sheets that detach along the ductile–brittle transition in either continental or oceanic crust, and (3) type F or fold-related crystalline thrust sheets that are generated beneath the ductile–brittle transition by plastically shearing the common limb between antiforms and/or synforms. The characteristics of these thrust sheets have been discussed in detail by Hatcher and Hooper (1992) and Hatcher (2004). Several individual structures are linked together in the Neka Valley in the outer parts of the Alborz foreland fold-and-thrust belt. The study nappe complex consists mainly of unmetamorphosed sedimentary rocks that display many buckles and chevron folds but few flow folds (except perhaps the nappe themselves). The Neka Valley nappe complex is part of a foreland fold-and-thrust nappe complex in an orogenic belt in which the thrusts propagate within a strongly anisotropic foreland-thinning wedge of layered sedimentary rocks that contains lithic units that are both weak and strong.

Among models of thrust nappes, the dominant process of nappe formation is the brittle and/or ductile accretion of tectonic units from a subducting plate into the overlying orogenic wedge by thrusting. Rocks of the Neka Valley nappe complex were not deformed very strongly during thrusting, strain pattern change systematically with structural and position, and obvious deformation is often confined to the basal thrust plane as in the Helvetic nappes of the European Alps (e.g. Zwart 1974), and the Willard thrust sheets of Idaho–Utah–Wyoming thrust belt (Yonkee 2005). This type of nappe tend to form at depths of less than ~5 km, and to be stacked in coherent piles of imbricate nappes. Such nappes range in size from mesoscopic (a few km long) to giants with strike lengths more than 700 km and their rheologies range from elastic to elastic–plastic (or even plastic) on the scale of the orogen (Chapple 1978; Hatcher 2004). The dominant deformation mechanism within foreland thrust sheets is the displacement of blocks of weakly deformed rock along discrete, mineral-coated minor faults (Wojtal 1986).

Conclusions

The magnitude of finite strain in the Neka Valley nappe complex is generally low, and its distribution is related to the Eo-Cimmerian deformation phase of the Alborz orogeny. Splays of reverse faults in the footwalls and hangingwalls of thrusts point to brittle deformation during thin-skinned tectonics. The nappes emplaced and subsequently deformed at temperatures just low enough to avoid metamorphosing the sediments. Heat produced due to deformation (Mukherjee and Mulchrone 2013; Mulchrone and Mukherjee 2015, 2016; Mukherjee 2016b) seems to be negligible. Subsequent thermal relaxation led to more brittle deformation during low-temperature dynamic metamorphism. The systematic variation of finite strain parameters (k, ν and ε_s) within the study area indicates heterogeneous simple shear and non-coaxial flattening. On the largest scale, the patterns of strain within the nappes in the eastern segment of the Alborz Mountain Range were probably regular. However, partitioning of the strain and its intensity on small scales was everywhere characterised by two heterogeneous effects. Plotting finite strains on the Flinn diagram suggests that a huge majority of the sediments in the fold-and-thrust belt flattened by oblate strain along a gentle SW–NE plane. This strain symmetry relates the ductile to brittle deformation during thrusting of the Khosh Yeilagh and Ruteh sequences over the Ghalemoran limestones along the Tertiary Talanbar and Haji-abad thrusts. This thrusting was followed by left-lateral strike-slip shear between these two formations. Such differential transport condition within nappe complex can develop perhaps beside sidewall ramps. Most ductile structures are overprinted by brittle structures. Structures such as orthogonal extensional joints striking NE–SW and NW–SE and pinch-and-swell structures in the west and east of the with steep ~NW–SE strike as tectonic transport parallel extension are compatible with diverging and parallel flow streamlines patterns of slowing flow accelerating to a steady shear flow.

Deformation can be coaxial in the slowing flow signalled by divergent streamlines but the strain path lies in the field of apparent flattening on the Flinn diagram (Fig. 8a–c). The axes of flow folds are generally at high angles perpendicular to the tectonic transport direction indicated by the streamlines mapped by any flow foliation. The cross-sectional area across the streamlines increases during divergent flow from NE to SE across the region (e.g. Hansen 1971). Divergent flow is recorded by orthogonal extension joints in the Qezel Qaleh Formation, orthogonal extensional fracture on the strike-slip fault plane in Ghalemoran Formation, and pinch-and-swell structures along the strike of the Ghalemoran Formation (Fig. 5). In shear flow signalled by parallel streamlines, the deformation is non-coaxial and the cross-sectional area remains constant. A vertical velocity gradient across a steady shear will induce non-coaxial deformation (Xypolias and Kokkalas 2006; Mukherjee 2012a, b). Field evidence for non-coaxial deformation in the Neka Valley nappe complex includes recumbent, asymmetric folds (e.g. Fossen and Rykkelid 1990; Fossen and Holst 1995; Carosi et al. 2004, 2005) and multiple generations of faults. In addition to the simple shear component, the local presence of upright folds demonstrates that there is a coaxial pure shear component in nappe emplacement mechanism. In that case, the coaxial strain includes a velocity gradient parallel to the direction flow (red lines in Fig. 6a).

The NE–SW strikes with NNW–NW dips of most of the faults in the Neka Valley confirm the southeastward tectonic transport direction of the allochthonous units in the eastern Alborz (e.g. Zwart 1974; Ramberg 1977). In addition, mesoscopic (~100 m) and large-scale (km) thrust slices with thrusts dipping uniformly north to northwest demonstrate a uniform top-to-southeast sense of tectonic transport and brittle–ductile shear in the study area (e.g. Mukherjee 2007, 2011a, b, 2012a, b).

Combining all the structural evidence of values of $k < 1$ and $\alpha < 1$ suggests to us that the dominant drive of emplacing the Neka Valley nappe complex was a rear compression (push from behind). In general, the forces driving the emplacement of any nappes affect the evolution of the regional structural patterns in both time and space. In other words, the rear compression emplacement mechanism in the study nappe complex is demonstrated by nappe complex thinning from the rear in the NW to the front in the SE. This arrangement could also be due to other emplacement mechanisms, such as gravity spreading or gliding from the NW to the SE. Both gravity spreading and gliding from the NW to the SE could have followed the collision between Iran and Eurasia and be a result of the subsequent NW–SE continental convergence over a horizontal no-slip basal boundary of an orogenic wedge with a foreland-inclined palaeoslope which is marked by a tank-track fold due frontal rolling (Brun and Merle 1985, 1988; Merle 1986; Talbot and Aftabi 2004; Talbot and Pohjola 2009; Baikpour and Talbot 2012; Nabavi 2012; Fig. 9c in Nabavi et al. 2016a).

The kinematic vorticity number (W_k) derived from our strain data is estimated to range from 0.4 to 0.85 with an average of $W_k = 0.6$. This implies that the NE arm of the Alborz orogeny underwent a general non-coaxial shear (e.g. Ring 1998; Mukherjee and Koyi 2010). The implication of our strain ellipsoids plotting in the field of apparent flattening, and of $S > L$ fabrics being the most common throughout the region is that the Neka Valley nappe complex is a zone of sinistral inclined transpression dominated by pure shear (Nabavi et al. 2014, Nabavi et al. 2016a).

The complex patterns in the parameters of finite strain which include variations in the magnitude of strains are due to strains partitioning on a range of different scales throughout the region. The patterns of finite strain within the Nake Valley nappe complex found here is consistent with Eo-Cimmerian transpression. There appears to have been little internal deformation within the Neka Valley nappe complex associated with such major thrusts as the Talanbar, Hajiabad, Radekan, Shah-Kuh and North Alborz thrust. As seen in the study of other mountain belts (e.g. Alps, Zagros), the study of finite strain of deformed objects can be a very helpful tool to better understand, interpret and analogue and or numerically model the nappe tectonics along the eastern branch of the Alborz Mountains. Brittle deformation (Babar et al. 2016; Kaplay et al. 2016, submitted; Misra et al. 2014; Misra and Mukherjee 2016) subsequent to ductile deformation usually does not alter strain analyses.

Acknowledgements We thank Prof. Christopher J. Talbot for helpful and constructive reviews, English language, and geological discussions that significantly improved this manuscript. In addition, we are grateful for the field assistance provided by MSc student Ali Shafiei. This work is supported by the Vice Presidency of Research and Technology of Golestan University Grant No. 1122. We would like to express our thanks to Dr. Soumyajit Mukherjee and Prof. Wolf-Christian Dullo for their careful handling of the manuscript.

References

Abad I, Gutiérrez-Alonso G, Nieto F et al (2003) The structure and the phyllosilicates (chemistry, crystallinity and texture) of Talas Ala-Tau (Tien Shan, Kyrgyz Republic): comparison with more recent subduction complexes. Tectonophysics 365:103–127

Abdelsalam MG (2010) Quantifying 3D post-accretionary tectonic strain in the Arabian-Nubian Shield: superimposition of the Oko Shear Zone on the Nakasib Suture, Red Sea Hills, Sudan. J Afr Earth Sc 56:167–178

Alavi M (1996) Tectonostratigraphic synthesis and structural style of the Alborz Mountain system in northen Iran. J Geodyn 21:1–33

Allen MB, Ghassemi MR, Shahrabi M et al (2003) Accommodation of late Cenozoic oblique shortening in the Alborz range, northern Iran. J Struct Geol 25:659–672

Allen MB, Jackson J, Walker R (2004) Late Cenozoic reorganization of the Arabia-Eurasia collision and the comparison of short-term and long-term deformation rates. Tectonics 23:1–16

Aoya M, Wallis SR (2003) Role of nappe boundaries in subduction-related regional deformation: spatial variation of meso- and microstructures in the Seba eclogite unit, the Sambagawa belt, SW Japan. J Struct Geol 25:1097–1106

Babar MD, Kaplay RD, Mukherjee S et al (2016) Evidences of deformation of dykes from Central Deccan Volcanic Province, Aurangabad, Maharashtra, India. In: Mukherjee S, Misra AA, Calvés G, Nemčok M (eds) Tectonics of the Deccan Large Igneous Province: an introduction. Geological Society of London, Special Publications. doi:10.1144/SP445.13

Baikpour S, Talbot CJ (2012) The Garmsar salt nappe and seasonal inversions of surrounding faults imaged by SAR interferometry, Northern Iran. Geol Soc Lond Spec Publ 363:563–578

Baird GB, Hudleston PJ (2007) Modelling the influence of tectonic extrusion and volume loss on the geometry, displacement, vorticity, and strain compatibility of ductile shear zones. J Struct Geol 29:1665–1678

Ballato P, Nowaczyk NR, Landgraf A et al (2008) Tectonic control on sedimentary facies pattern and sediment accumulation rates in the Miocene foreland basin of the southern Alborz mountains, northern Iran. Tectonics 27:1–20

Ballato P, Uba CE, Landgraf A et al (2011) Arabia-Eurasia continental collision: insights from the Tertiary foreland-basin evolution in the Alborz mountains, northern Iran. Geol Soc Am Bull 123:106–131

Berberian M, King GC (1981) Toward a paleogeography and tectonic evolution of Iran. Can J Earth Sci 18:210–265

Bhattacharyya P, Hudleston PJ (2001) Strain in ductile shear zones in the Caledonides of northern Sweden; a three-dimensional puzzle. J Struct Geol 23:1549–1556

Bhattacharyya K, Mitra G (2009) A new kinematic evolutionary model for the growth of a duplex—an example from the Rangit duplex, Sikkim Himalaya, India. Gondwana Res 16:697–715

Biswas T, Dutta D, Mukherjee S (2014) Tectonics of Siwalik Himalaya in Dehradun-Roorkee section, India. Geological Society of America annual meeting in Vancouver, British Columbia (19–22 October 2014). Topical session: T.23 Exploring the Development of the Himalayan-Karakoroum-Tibet Orogenic System from the Mantle to Mountain Peaks

Bose N, Mukherjee S (2015) Back structures (back-fault and back-folds) from collisional orogeny: field findings from Lesser Himalaya, Sikkim, India. 30th Himlaya-Karakoram-Tibet Workshop, Wadia Institute of Himalayan Geology, 06–08 Oct, Dehradun, India, pp 13–14

Brandon MT (1995) Analysis of geologic strain data in strain-magnitude space. J Struct Geol 17:1375–1385

Brun JP, Merle O (1985) Strain pattern in models of spreading-gliding nappes. Tectonics 4:705–719

Brun JP, Merle O (1988) Experiments on folding in spreading-gliding nappes. Tectonophysics 145:129–139

Burg J-P, Ricou L-E, Ivanov Z et al (1996) Syn-metamorphic nappe complex in the Rhodope Massif. Structure and kinematics. Terra Nova 8:6–15

Capponi G, Carosi R, Meccheri M et al (2003) Strain analysis in the Millen Range of Northern Victoria Land, Antarctica. Geol Jahrb B 85:225–251

Carosi R, Iacopini D, Montomoli C (2004) Asymmetric fold development in the Variscan Nappes. CR Geosci 336:939–949

Carosi R, Frassi C, Montomoli C et al (2005) Structural evolution of the Tuscan Nappe in the southeastern sector of the Apuan Alps metamorphic dome (Northern Apennines, Italy). Geol J 40:103–119

Carosi R, Addario E, Mammoliti E et al (2016) Geology of the northwestern portion of the Ferriere-Mollieres Shear Zone, Argentera Massif, Italy. J Maps. doi:10.1080/17445647.2016.1243491

Cello G, Nur A (1988) Emplacement of foreland thrust systems. Tectonics 7:261–271

Chapple WM (1978) Mechanics of thin-skinned fold-and-thrust belts. Geol Soc Am Bull 93:1189–1198

Coward MP (1976) Strain within ductile shear zones. Tectonophysics 34:181–197

Coward MP (1980) The Caledonian thrust and shear zones of N.W. Scotland. J Struct Geol 2:11–17

Coward MP, Kim JH (1981) Strain within thrust sheets. In: McClay KR, Price NJ (eds) Thrust and nappe tectonics. Geological Society of London, Special Publications 9, pp 275–292

Czeck DM, Hudleston PJ (2003) Testing models for obliquely plunging lineation in transpression: a natural example and theoretical discussion. J Struct Geol 25:959–982

Dahlen FA, Suppe J, Davis D (1984) Mechanics of fold-and-thrust belts and accretionary wedges: cohesive Coulomb theory. J Geophys Res 89:1189–1198

Davis DM, Engelder T (1985) The role of salt in fold-and-thrust belts. Tectonophysics 119:67–88

Davis DM, Lillie RJ (1994) Changing mechanical response during continental collision: active examples from the foreland thrust belts of Pakistan. J Struct Geol 16:21–34

Dias R, Mateus A, Ribeiro A (2003) Strain partitioning in transpressive shears zones in the southern branch of the Variscan Ibero-Armorican arc. Geodin Acta 16:119–129

Djamour Y, Vernant P, Bayer R et al (2010) GPS and gravity constraints on continental deformation in the Alborz mountain range, Iran. Geophys J Int 183:1287–1301

Dubey AK (2014) Understanding an orogenic belt: structural evolution of the Himalaya. Springer, New York

Elliott D (1976) The motion of thrusts sheets. J Geophys Res 81:949–963

Epard J-L, Escher A (1996) Transition from basement to cover: a geometric model. J Struct Geol 18:533–548

Escher A, Masson H, Steck A (1993) Nappe geometry in the Western Alps. J Struct Geol 15:501–509

Eyster EL, Bailey CM (2001) Vorticity analyses of extensional and transpressional high-strain zones; examples from the Arizona basin and range and Virginia piedmont. Geol Soc Am Abstr Prog 33(2):5

Fissler DA (2006) A quantitative analysis of strain in the Seine River Meta-conglomerates, Rainy Lake region, Northwestern Ontario, Canada. Unpublished M.S. thesis. University of Wisconsin-Milwaukee

Flinn D (1956) On the deformation of the funzie conglomerate, Feltar, Shetland. J Geol 64:480–505

Flinn D (1962) On folding during three-dimensional progressive deformation. Q J Geol Soc 118:385–428

Flinn D (1979) The deformation matrix and the deformation ellipsoid. J Struct Geol 1:299–307

Fossen H (1993a) Linear fabrics in the Bergsdalen Nappes, southwest Norway: implications for deformation history and fold development. Nor Geol Tidsskr 73:95–108

Fossen H (1993b) Structural evolution of the Bergsdalen Nappes, Southwest Norway. Norsk Geol Unders Bull 424:23–49

Fossen H (2016) Structural geology, 2nd edn. Cambridge University Press, Cambridge

Fossen H, Holst TB (1995) Northwest-verging folds and the northwestward movement of the Caledonian Jotun Nappe, Norway. J Struct Geol 17:3–15

Fossen H, Rykkelid E (1990) Shear zone structures in the Øygarden area, West Norway. Tectonophysics 174:385–397

Fossen H, Tikoff B (1993) The deformation matrix for simultaneous simple shearing, pure shearing and volume change, and its application to transpression-transtension tectonics. J Struct Geol 15(3–5):413–422
Fowler A, El Kalioubi B (2004) Gravitational collapse origin of shear zones, foliations, and linear structures in the Neoproterozoic cover nappes, Eastern Desert, Egypt. J Afr Earth Sci 38:23–40
Frehner M (2011) The neutral lines in buckle folds. J Struct Geol 33(10):1501–1508
Frehner M (2016) 3D fold growth in transpression. Tectonophysics. doi:10.1016/j.tecto.2016.01.002
Frehner M, Exner U (2014) Strain and foliation refraction patterns around buckle folds. Geol Soc Lond Spec Publ 394:21–37
Fry N (1979) Random point distribution and strain measurements. Tectonophysics 60:89–105
Gee DG (1978) Nappe emplacement in the Scandinavian Caledonides. Tectonophysics 47:393–419
Gray DR (1995) Thrust kinematics and transposition fabrics from a basal detachment zone, eastern Australia. J Struct Geol 17:1637–1654
Gray DR, Willman CE (1991) Thrust-related strain gradient and thrusting mechanisms in a chevron-folded sequence, southern Australia. J Struct Geol 13:691–710
Groshong RH Jr, Pfiffner OA, Pringle LR (1984) Strain partitioning in the Helvetic thrust belt of eastern Switzerland from the leading edge to the internal zone. J Struct Geol 6:5–18
Guest B, Guest A, Axen G (2007) Late Tertiary tectonic evolution of northern Iran: a case for simple crustal folding. Glob Plan Change 58:435–453
Guillier B (1988) Modélisation analogique des interactions compression gravite. Diplômed'Etude Approfondie, Rennes
Gutiérrez-Alonso G (1996) Strain partitioning in the footwall of the Somiedo Nappe: structural evolution of the Narcea Tectonic Window, NW Spain. J Struct Geol 18:1217–1229
Hansen EC (1971) Strain facies. Springer, New York
Harris LB, Burg J-P, Sauniac S (1983) Strain distribution within the Pardailhan Nappe (Montagne Noire, France) and structure of its basal thrust zone: implication for events associated with nappe emplacement. J Struct Geol 5:431–440
Hatcher RD Jr (2004) Properties of thrusts and the upper bounds for the size of thrust sheets. In: McClay KR (ed) Thrust tectonics and hydrocarbon systems. American Association of Petroleum Geologists Memoir 82, pp 18–29
Hatcher RD Jr, Hooper RJ (1992) Evolution of crystalline thrust sheets in the internal parts of mountain chains. In: McClay KR (ed) Thrust tectonics. Chapman and Hall, London, pp 217–233
Henderson GGL, Dahlstom DCA (1959) First-order nappe in Canadian Rochies. Am Assoc Petrol Geol Bull 43(3):641–653
Hollinsworth J, Jackson J, Walker R et al (2008) Extrusion tectonics and subduction in the eastern South Caspian region since 10 Ma. Geology 36:763–766
Hossack J (1968) Pebble deformation and thrusting in the Bygdin area (Southern Norway). Tectonophysics 5:315–339
Hsu TC (1966) The characteristics of coaxial and non-coaxial strain paths. J Strain Anal Eng Des 1:216–222
Hsü KJ (1969) Role of cohesive strength in the mechanics of overthrust faulting and of landsliding. Geol Soc Am Bull 80:927–952
Hubbert MK, Rubey WW (1959) Role of fluid pressure in mechanics of overthrust faulting, I. Mechanics of fluid-filled porous solids and its application to overthrust faulting. Geol Soc Am Bull 70:115–166
Hudleston PJ (1976) Recumbent folding in the base of the Barnes ice cap, Baffin Island, northwest Territories, Canada. Geol Soc Am Bull 87:1684–1692
Hudleston PJ (1977) Similar folds, recumbent folds and gravity tectonics in ice and rocks. J Geol 85:113–122
Hudleston PJ (2015) Structures and fabrics in glacial ice: a review. J Struct Geol 81:1–27
Hudleston PJ, Hooke R (1980) Cumulative deformation in the Barnes ice cap and implications for the development of foliation. Tectonophysics 66:127–146
Jackson J, McKenzie D (1984) Active tectonics of the Alpine-Himalayan Belt between western Turkey and Pakistan. Geophys J Int 77:185–264
Jackson J, Priestley K, Allen MB et al (2002) Active tectonics of the South Caspian Basin. Geophys J Int 148:214–245
Javidfakhr B, Bellier O, Shabanian S et al (2011) Plio-Quaternary tectonic regime changes in the transition zone between Alborz and Kopeh Dagh mountain ranges (NE Iran). Tectonophysics 506:86–108
Jordan P (1992) Evidence for large-scale decoupling in the Triassic evaporates of Northern Switzerland: an overview. Eclogae Geol Helv 85:677–693
Kaplay RD, Babar Md, Mukherjee S et al (2016) Morphotectonic expression of geological structures in eastern part of south east Deccan volcanic province (around Nanded, Maharashtra, India). In: Mukherjee S, Misra AA, Calvés G, Nemčok M (eds) Tectonics of the Deccan Large Igneous Province: an introduction. Geological Society of London, Special Publications. doi:10.1144/SP445.12
Kaplay RD, Kumar TV, Mukherjee S et al (submitted) Strike-slip (brittle/brittle-ductile) shear from the periphery of South East Deccan Volcanic Province, Kinwat, Maharashtra, India. J Earth Syst Sci
Kassem OMK, Abd El Rahim SH (2010) Finite-strain analysis of Metavolcano-sedimentary rocks at Gabel El Mayet area, Central Eastern Desert, Egypt. J Afr Earth Sci 58:321–330
Kehle RO (1970) Analysis of gravity sliding and orogenic translation. Geol Soc Am Bull 81:1641–1664
Kligfield R, Carmignani L, Owens WH (1981) Strain analysis of a Northern Apennine shear zone using deformed marble breccias. J Struct Geol 16:493–503
Lagarde JL, Michard A (1986) Stretching normal to the regional thrust displacement in a thrust-wrench shear zone, Rehamna Massif, Morocco. J Struct Geol 8:483–492
Long S, McQuarrie N, Tobgay T et al (2011) Quantifying internal strain and deformation temperature in the eastern Himalaya, Bhutan: implications for the evolution of strain in thrust sheets. J Struct Geol 33:579–608
McClay KR (1992) Glossary of thrust tectonics terms. In: McClay KR (ed) thrust tectonics. Chapman & Hall, London, pp 419–433
McClay KR, Price NJ (1981) Introduction. In: McClay KR, Price NJ (eds) Thrust and nappe tectonics. Geological Society of London, Special Publications 9, pp 1–9
Merle O (1986) Patterns of stretch trajectories and strain rate within spreading-gliding nappes. Tectonophysics 124:211–222
Merle O (1989) Strain models within spreading nappes. Tectonophysics 165:57–71
Merle O (1998) Emplacement mechanisms of nappes and thrust sheets. Kluwer Academic Publishers, Dordrecht
Merle O, Brun J-P (1984) The curved translation path of the Parpaillon nappe (French Alps). J Struct Geol 6:711–719
Misra AA, Mukherjee S (2016) Dyke-brittle shear relationships in the Western Deccan Strike-slip Zone around Mumbai (Maharashtra, India). In: Mukherjee S, Misra AA, Calvés G, Nemčok M (eds) Tectonics of the Deccan Large Igneous Province: an introduction. Geological Society of London, Special Publications. doi:10.1144/SP445.4
Misra AA, Bhattacharya G, Mukherjee S et al (2014) Near N–S paleo-extension in the western Deccan region in India: does

it link strike-slip tectonics with India-Seychelles rifting? Int J Earth Sci 103:1645–1680
Mitra G (1994) Strain variation in thrust sheets across the Sevier fold-and-thrust belt (Idaho–Utah–Wyoming): implication for section restoration and wedge taper evolution. J Struct Geol 16:585–602
Mitra G, Boyer SE (1999) Strain in the Lewis thrust sheet, NW Montana fold-and-thrust belt: implications for basin restoration and estimates of critical taper. Geol Soc Am Abstr Prog 31:237
Moriyama Y, Wallis SR (2002) Three-dimensional finite strain analysis in the high-grade part of the Sanbagawa Belt using deformed meta-conglomerate. Isl Arc 11:111–121
Mukherjee S (2005) Channel flow, ductile extrusion and exhumation of lower-mid crust in continental collisional zones. Curr Sci 89:435–436
Mukherjee S (2007) Geodynamics, deformation and mathematical analysis of metamorphic belts of the NW Himlaya. Unpublished Ph.D. thesis. Indian Institute of Technology, Roorkee
Mukherjee S (2010a) Applicability of channel flow as an extrusion mechanism of the Higher Himalayan Shear Zone from Sutlej, Zanskar, Dhauliganga and Goriganga Sections, Indian Himalaya. European Geosciences Union General Assembly, 2–7 May, 2010, Vienna, Austria. Geophysical Research Abstracts, vol 12, EGU2010-14
Mukherjee S (2010b) Microstructures of the Zanskar Shear Zone. Earth Sci India 3:9–27
Mukherjee S (2010c) Structures at Meso- and Micro-scales in the Sutlej section of the Higher Himalayan Shear Zone in Himalaya. E-Terra 7:1–27
Mukherjee S (2011a) Flanking microstructures from the Zanskar Shear Zone, NW Indian Himalaya. YES Netw Bull 1:21–29
Mukherjee S (2011b) Mineral fish: their morphological classification, usefulness as shear sense indicators and genesis. Int J Earth Sci 100:1303–1314
Mukherjee S (2012a) Simple shear is not so simple! Kinematics and shear senses in Newtonian viscous simple shear zones. Geol Mag 149:819–826
Mukherjee S (2012b) Tectonic implications and morphology of trapezoidal mica grains from the Sutlej section of the Higher Himalayan Shear Zone, Indian Himalaya. J Geol 120:575–590
Mukherjee S (2013a) Channel flow extrusion model to constrain dynamic viscosity and Prandtl number of the Higher Himalayan Shear Zone. Int J Earth Sci 102:1811–1835
Mukherjee S (2013b) Deformation microstructures in rocks. Springer, New York
Mukherjee S (2013c) Higher Himalaya in the Bhagirathi section (NW Himalaya, India): its structures, back-thrusts and extrusion mechanism by both channel flow and critical taper mechanisms. Int J Earth Sci 102:1851–1870
Mukherjee S (2014a) Atlas of shear zone structures in meso-scale. Springer, New York
Mukherjee S (2014b) Kinematics of 'top-to-down' simple shear in a Newtonian Rheology. J Indian Geophys Union 18:245–248
Mukherjee S (2014c) Mica inclusion inside Host Mica Grains from the Sutlej Section of the Higher Himalayan Crystallines, India-Morphology and Constrains in Genesis. Acta Geol Sin 88:1729–1741
Mukherjee S (2014d) Review of flanking structures in meso- and micro-scales. Geol Mag 151:957–974
Mukherjee S (2015) A review on out-of-sequence deformation in the Himalaya. In: Mukherjee S, Carosi R, van der Beek P, Mukherjee BK, Robinson D (eds) Tectonics of the Himalaya. Geological Society, London, Special Publications 412, no 1, pp 67–109
Mukherjee S (2016a) Review on symmetric structures in ductile shear zones. Int J Earth Sci. doi:10.1007/s00531-016-1366-4
Mukherjee S (2016b) Shear heating by translational brittle reverse faulting along a single, sharp and straight fault plane. J Earth Syst Sci
Mukherjee S, Biswas R (2014) Kinematics of horizontal simple shear zones of concentric arcs (Taylor–Couette flow) with incompressible Newtonian rheology. Int J Earth Sci 103:597–602
Mukherjee S, Koyi HA (2010) Higher Himalayan Shear Zone, Sutlej section: structural geology and extrusion mechanism by various combinations of simple shear, pure shear and channel flow in shifting modes. Int J Earth Sci 99:1267–1303
Mukherjee S, Mulchrone KF (2013) Viscous dissipation pattern in incompressible Newtonian simple shear zones: an analytical model. Int J Earth Sci 102:1165–1170
Mukherjee S, Koyi HA, Talbot CJ (2012) Implications of channel flow analogue models in extrusion of the Higher Himalayan Shear Zone with special references to the out-of-sequence thrusting. Int J Earth Sci 101:253–272
Mukherjee S, Punekar J, Mahadani T et al (2015) A review on intrafolial folds and their morphologies from the detachments of the western Indian Higher Himalaya. In: Mulchrone K, Mukherjee S (eds) Ductile shear zones: from micro- to macro-scales. Wiley, New York, pp 182–205
Mulchrone KF, Mukherjee S (2015) Shear senses and viscous dissipation of layered ductile simple shear zones. Pure Appl Geophys 172:2635–2642
Mulchrone KF, Mukherjee S (2016) Kinematics and shear heat pattern of ductile simple shear zones with 'slip boundary condition'. Int J Earth Sci 105:1015–1020
Nabavi ST (2012) Emplacement mechanism of fold-and-thrust nappes in Chahar-bagh area, Eastern Alborz. Unpublished M.Sc. thesis. Damghan University, Iran **(in Persian with English abstract)**
Nabavi ST, Khademi M, Rahimi-Chakdel A (2014) Inclined transpression deformation zone of Chahr-bagh nappe, eastern Alborz. J Tecton Struct 2:56–76 **(In Persian with English abstract)**
Nabavi ST, Díaz-Azpíroz M, Talbot CJ (2016a) Inclined transpression in the Neka Valley, eastern Alborz, Iran. Int J Earth Sci. doi:10.1007/s00531-016-1388-y
Nabavi ST, Alavi SA, Mohammadi S, Ghassemi MR, Shirzaei M (2016b) Analysis of transpression within contractional planar fault steps using the finite-element method. Geological Society of America Abstracts with Programs, vol 48, no 7. doi:10.1130/abs/2016AM-280211
Nadai A (1963) Theory of flow and fracture of solids, vol 2. McGraw-Hill, New York
O'Hara KD (1990) State of strain in mylonites from the western Blue Ridge province, south Appalachians: the role of volume loss. J Struct Geol 12:419–430
Owens WH (1984) The calculation of a best-fit ellipsoid from elliptical sections on arbitrarily oriented planes. J Struct Geol 6:571–578
Pastor-Galán D, Gutiérrez-Alonso G, Meere PA et al (2009) Factors affecting finite strain estimation in low-grade, low-strain clastic rocks. J Struct Geol 31:1586–1596
Pfiffner OA (1981) Fold-and-thrust tectonics in the Helvetic Nappes (E Switzerland). In: McClay KR, Price NJ (eds) Thrust and nappee tectonics. Geological Society, London, Special Publications 9, no 1, pp 319–327
Pfiffner OA (1985) Displacements along thrust faults. Eclogae Geol Helv 78:313–333
Pfiffner OA (1993) The structure of the Helvitic nappes and its relation to the mechanical stratigraphy. J Struct Geol 15(3–5):511–521
Pfiffner OA (2006) Thick-skinned and thin-skinned styles of continental contraction. In: Mazzoli S, Butler RWH (eds) Styles of continental contraction. Geological Society of America, Special Paper 414, pp 153–177

Plašienka D, Prokešova R (1996) Towards an evolutionary tectonic model of the Krížna cover nappe (Western Carpathians, Slovakia). Slovak Geol Mag 3–4(96):279–286
Platt JP (1986) Dynamics of orogenic wedges and the uplift of high-pressure metamorphic rocks. Geol Soc Am Bull 97:1037–1053
Prokešova R, Plašienka D, Milovský R (2012) Structural pattern and emplacement mechanisms of the Krížna cover nappe (Central Western Carpathians). Geol Carpath 63:13–32
Provost A, Buisson C, Merle O (2004) From progressive to finite deformation and back. J Geophys Res. doi:10.1029/2001JB001734
Rahimi-Chakdel A, Raghimi M (2014) Some characteristics of mafic dykes in Gondwanan land from South of Gorgan, Northeastern Iran: implication to Petrogenesis and Paleotectonic. J Tethys 2:137–147
Ramberg H (1975a) Particle path, displacement and progressive strain applicable to rocks. Tectonophysics 28:1–37
Ramberg H (1975b) Superposition of homogeneous strain and progressive deformation in rocks. Bull Geol Inst Univ Uppsala NS 6:35–67
Ramberg H (1977) Some markers on the mechanism of nappe movement. Geol Fören Stockh Förh 99:110–117
Ramberg H (1989) A new numerical simulation method applied to spreading nappes. Tectonophysics 162:173–192
Ramberg H (1991) Numerical simulation of spreading nappes, sliding against basal friction. Tectonophysics 188:159–186
Ramsay JG (1967) Folding and fracturing of rocks. McGraw-Hill, New York
Ramsay JG (1981) Tectonics of the Helvetic Nappes. In: McClay KR, Price NJ (eds) Thrust and nappee tectonics. Geological Society, London, Special Publications 9, no 1, pp 293–309
Ramsay JG, Huber MI (1983) The techniques of modern structural geology: strain analysis, vol 1. Academic Press, London
Ramsay JG, Wood DS (1973) The geometric effects of volume change during deformation processes. Tectonophysics 16:263–277
Ring U (1998) Volume strain, strain type and flow path in a narrow shear zone. Geol Rundsch 86:786–801
Ring U, Kassem OMK (2007) The nappe rule: why does it work? J Geol Soc Lond 164:1109–1112
Ring U, Bradon MT, Ramthum A (2001) Solution mass-transfer deformation adjacent to the Glarus Thrust, with implications for the tectonic evolution of the Alpine wedge in eastern Switzerland. J Struct Geol 23:1491–1505
Ritz JF, Nazari H, Ghassemi A et al (2006) Active transtension inside Central Alborz: a new insight into northern Iran-southern Caspian geodynamics. Geology 34:477–480
Roday P, Purohit MK, Prajapati KK (2010) A compute program for the determination of finite strain using Fry method. J Geol Soc India 76:151–154
Samani B (2015) Strain analysis using structural elements and geometry of surfaces of no finite longitudinal strain. Arab J Geosci 8:8461–8468
Sanderson DJ (1982) Models of strain variation in nappes and thrust sheets: a review. Tectonophysics 88:201–233
Sanderson DJ, Marchini WRD (1984) Transpression. J Struct Geol 6:449–458
Sanderson DJ, Andrew JR, Phollips WEA et al (1980) Deformation studies in the Irish Caledonides. J Geol Soc Lond 137:289–302
Sarkarinejad K, Samani B, Faghih A et al (2010) Implication of strain and vorticity of flow analyses to interpret the kinematics of an oblique convergence event Zagros Mountains, Iran). J Asian Earth Sci 38:34–43
Sarkarinejad K, Keshavarz S, Faghih A (2015) Kinematics of the Sirjan mylonite nappe, Zagros Orogenic Belt: insights from strain and vorticity analyses. J Geosci 60:189–202
Schmalholz SM, Duretz T, Schenker FL et al (2014) Kinematics and dynamics of tectonic nappes: 2-D numerical modelling and implications for high and ultra-high pressure tectonism in the Western Alps. Tectonophysics 631:160–175
Seno S (1992) Finite strain and deformation within the Briançonnais Castelvecchio-Cerisola nappe of the Ligurian Alps, Italy. J Struct Geol 14:825–838
Seno S, Dallagiovanna G, Vanossi M (1998) From finite strain data to strain history: a model for a sector of the Ligurian Alps, Italy. J Struct Geol 20:573–585
Shahrabi M (1990) Geological map of the gorgan quadrangle, scale: 1:250,000. Geological Survey of Iran, Tehran
Siddans AWB (1983) Finite strain patterns in some Alpine nappes. J Struct Geol 5:441–448
Siddans AWB (1984) Thrust tectonics—a mechanistic view from the West and Central Alps. Tectonophysics 104:257–281
Siddans AWB, Henry B, Kligfield R et al (1984) Finite strain patterns and their significance in Permian rocks of the Alpes Maritimes (France). J Struct Geol 6:339–368
Singh S, Jain AK (1993) Deformational and strain patterns of the Jutogh Nappe along the Sutlej Valley in Jeori-Wangtu region, Himachal Pradesh, India. J Himal Geol 4:41–55
Talbot CJ (1974) Fold nappes as asymmetric mantled gneiss domes and ensialic orogeny. Tectonophysics 24:259–276
Talbot CJ (1979) Fold trains in a glacier of salt in southern Iran. J Struct Geol 1(1):5–18
Talbot CJ (2014) Lessons from the first 100 minimum strain ellipsoids constrained in gneisses deformed at high metamorphic grade. Earth Sci Rev 138:231–267
Talbot CJ, Aftabi P (2004) Geology and models of salt extrusion at Qum Kuh, central Iran. J Geol Soc Lond 161:321–334
Talbot CJ, Pohjola V (2009) Subaerial salt extrusions in Iran as analogues of ice sheets, streams and glaciers. Earth Sci Rev 97:167–195
Talbot CJ, Sokoutis D (1995) Strain ellipsoids from incompetent dykes: application to volume loss during mylonitization in the Singo gneiss zone, central Sweden. J Struct Geol 17:927–948
Thigpen JR, Law RD, Lloyd GE et al (2010) Deformation temperatures, vorticity of flow and strain in the Moine thrust zone and Moine nappe: reassessing the tectonic evolution of the Scandian foreland-hinterland transition zone. J Struct Geol 32:920–940
Tikoff B, Fossen H (1993) Simultaneous pure and shear shear: the unifying deformation matrix. Tectonophysics 217:267–283
Toriumi M (1985) Two type of ductile deformation/regional metamorphic belt. Tectonophysics 113:307–326
Toriumi M, Noda H (1986) The origin of strain patterns resulting from contemporaneous deformation and metamorphism in the Sambagawa metamorphic belt. J Metamorph Geol 4:409–420
Tripathy NR, Srivastava HB, Mamtani MA (2009) Evaluation of a regional strain gradient in mylonitic quartzites from the footwall of the Main Central Thrust Zone (Garhwal Himalaya, India): Inferences from finite strain and AMS analyses. J Asian Earth Sci 34:26–37
Twiss RJ, Moores EM (2007) Structural Geology, 2nd edn. Freeman and Company, New York
Vitale S, Mazzoli S (2008) Heterogeneous shear zone evolution: the role of shear strain hardening/softening. J Struct Geol 30:1363–1395
Vitale S, Mazzoli S (2009) Finite strain analysis of a natural ductile shear zone in limestones: Insights into 3-D coaxial vs. noncoaxial deformation partitioning. J Struct Geol 31:104–113
Vitale S, Mazzoli S (2010) Strain analysis of heterogeneous ductile shear zones based on the attitudes of planar markers. J Struct Geol 32:321–329
Vitale S, Mazzoli S (2015) From finite to incremental strain: insights into heterogeneous shear zone evolution. In: Mulchrone K, Mukherjee S (eds) Ductile shear zones: from micro- to macroscales. Wiley, New York, pp 3–13

Wallis SR (1995) Vorticity analysis and recognition of ductile extension in the Sanbagawa belt, SW Japan. J Struct Geol 17:1077–1093
Wissing SB, Pfiffner OA (2003) Numerical models for the control of inherited basin geometries on structures and emplacement of the Klippen nappe (Swiss Prealps). J Struct Geol 25:1213–1227
Wissing SB, Ellis S, Pfiffner OA (2003) Numerical models of Alpine-type cover nappes. Tectonophysics 367:145–172
Wojtal S (1986) Deformation within foreland thrust sheets by populations of minor faults. J Struct Geol 8:341–360
Xypolias P, Kokkalas S (2006) Heterogeneous ductile deformation along a mid-crustal extruding shear zone: an example from the External Hellenides (Greece). In: Law RD, Searle MP Godin L (eds) Channel flow, ductile extrusion and exhumation in continental collision zones. Geological Society, London, Special Publications 268, no 1, pp 497–516
Yonkee WA (2005) Strain patterns within part of the Willard thrust sheet, Idaho-Wyoming-Utah thrust belt. J Struct Geol 27:1315–1343
Yonkee WA, Czeck DM, Nachbor AC et al (2013) Strain accumulation and fluid-rock interaction in a naturally deformed diamictite, Willard thrust system, Utah (USA): implications for crustal theology and strain softening. J Struct Geol 50:91–118
Zanchi A, Berra F, Mattei M et al (2006) Inversion tectonics in Central Alborz, Iran. J Struct Geol 28:2023–2037
Zanchi A, Zanchetta S, Berra F, Mattei M, Garzanti E, Molyneux S, Nawab A, Sabouri J (2009) The Eo-Cimmerian (Late? Triassic) orogeny in North Iran. In: Brunet M-F, Wilmsen M, Granath JW (eds) South caspian to central Iran basins. The Geological Society, London, Special Publications 312, no 1, pp 31–55
Zwart HJ (1974) Structure and metamorphism in the Seve-Köli nappe complex (Scandinavian Caledonides) and its implications concerning the formation of metamorphic nappes. Centenaire de la Géologique de Belgique, Géologie des Domaines Cristallins, Liege, pp 129–144